The Journal of Immunology

Enhanced Nerve–Mast Cell Interaction by a Neuronal Short Isoform of Cell Adhesion Molecule-1

Man Hagiyama, Tadahide Furuno, Yoichiroh Hosokawa, Takanori Iino, Takeshi Ito, Takao Inoue, Mamoru Nakanishi, Yoshinori Murakami and Akihiko Ito

J Immunol 2011; 186:5983-5992; Prepublished online 11 April 2011;
doi: 10.4049/jimmunol.1002244
http://www.jimmunol.org/content/186/10/5983

The Journal of Immunology is published twice each month by
The American Association of Immunologists, Inc.,
1451 Rockville Pike, Suite 650, Rockville, MD 20852

Print ISSN: 0022-1767 Online ISSN: 1550-6606.

Enhanced Nerve–Mast Cell Interaction by a Neuronal Short Isoform of Cell Adhesion Molecule-1

Man Hagiyama,* Tadahide Furuno,† Yoichiroh Hosokawa,‡ Takanori Iino,‡ Takeshi Ito,* Takao Inoue,§ Mamoru Nakanishi,† Yoshinori Murakami,* and Akihiko Ito§

Close apposition of nerve and mast cells is viewed as a functional unit of neuro-immune mechanisms, and it is sustained by *trans*-homophilic binding of cell adhesion molecule-1 (CADM1), an Ig superfamily member. Cerebral nerve–mast cell interaction might be developmentally modulated, because the alternative splicing pattern of four (a–d) types of CADM1 transcripts drastically changed during development of the mouse cerebrum: developing cerebrums expressed CADM1b and CADM1c exclusively, while mature cerebrums expressed CADM1d additionally and predominantly. To probe how individual isoforms are involved in nerve–mast cell interaction, Neuro2a neuroblastoma cells that express CADM1c endogenously were modified to express additionally either CADM1b (Neuro2a-CADM1b) or CADM1d (Neuro2a-CADM1d), and they were cocultured with mouse bone marrow-derived mast cells (BMMCs) and BMMC-derived cell line IC-2 cells, both of which expressed CADM1c. BMMCs were found to adhere to Neuro2a-CADM1d neurites more firmly than to Neuro2a-CADM1b neurites when the adhesive strengths were estimated from the femtosecond laser-induced impulsive forces minimally required for detaching BMMCs. GFP-tagging and cross-linking experiments revealed that the firmer adhesion site consisted of an assembly of CADM1d *cis*-homodimers. When Neuro2a cells were specifically activated by histamine, intracellular Ca^{2+} concentration was increased in 63 and 38% of CADM1c-expressing IC-2 cells that attached to the CADM1d assembly site and elsewhere, respectively. These results indicate that CADM1d is a specific neuronal isoform that enhances nerve–mast cell interaction, and they suggest that nerve–mast cell interaction may be reinforced as the brain grows mature because CADM1d becomes predominant. ***The Journal of Immunology*****, 2011, 186: 5983–5992.**

Mast cells are normally resident in a variety of systemic organs and tissues, including intestinal and respiratory mucosa, skin dermis, dura mater, and cerebrum (1–4). Their distribution is seemingly at random, but closer observation reveals that mast cells prefer to locate around vessels and nerves and some of them are apparently in contact with nerve fibers (5). Electron microscopically, the most closely proximate areas between nerve and mast cells are composed of a parallel-aligned membrane–membrane apposition with a spatial gap of 20 nm or less (6, 7). These anatomical findings are suggestive of functional communication between nerve and mast cells that depends on cell–cell adhesion. Several lines of evidence support this suggestion at molecular levels: 1) neurites in contact with mast cells often contain neuropeptides, such as substance P and calcitonin gene-related peptide, and release these neuropeptides on stimulation (8, 9); and 2) mast cells express cognate receptors for various kinds of neuropeptides (10–13). Actually, trigeminal sensory nerve stimulation is reported to result in dura mater mast cell activation, that is, degranulation or secretion of mediators (14). In contrast, mast cells synthesize and release a variety of molecules, which can, in turn, influence neuronal activity (15, 16). For example, tryptase directly activates proteinase-activated receptors on neurons (17), and TNF-α and nerve growth factor can cause local nerves to be excited at lower threshold (18, 19). These nerve–mast cell crosstalks are assumed to play a role in the pathogenesis of many inflammatory diseases, such as atopic dermatitis, alopecia, asthma, and irritable bowel syndrome (20–22).

In an attempt to probe molecular mechanisms of nerve–mast cell interaction, we have been using a coculture system, in which bone marrow-derived cultured mast cells (BMMCs) and BMMC-derived cell line IC-2 cells are cultured on neurite networks sprouting out from superior cervical ganglion (SCG) neurons (23–25). This coculture is regarded as a reproductive model of anatomical and functional relationship between nerve and mast cells, because BMMCs or IC-2 cells adhere to SCG neurites, and IC-2 cells can communicate with neurites in a cell–cell adhesion-dependent manner (25). In 2003, we identified a new mast-cell adhesion molecule, named cell adhesion molecule-1 (CADM1) (26), and we subsequently identified that CADM1 was also expressed by SCG neurons and it bound homophilically in *trans* (25, 27). Based on these characteristics, CADM1 was found to make a crucial contribution to the adhesion of BMMCs or IC-2 cells to SCG neurites via *trans*-homophilic binding (25). Additionally, we revealed that CADM1 binding between SCG neurites and IC-2 cells resulted in promotion of communication between

*Division of Molecular Pathology, Institute of Medical Science, The University of Tokyo, Minato-ku, Tokyo 108-8639, Japan; †School of Pharmacy, Aichi Gakuin University, Nagoya, Aichi 464-8650, Japan; ‡Graduate School of Materials Science, Nara Institute of Science and Technology, Ikoma, Nara 630-0192, Japan; and §Department of Pathology, Faculty of Medicine, Kinki University, Osaka-Sayama, Osaka 589-8511, Japan

Received for publication July 14, 2010. Accepted for publication March 11, 2011.

This work was supported by grants from the Ministry of Education, Culture, Sports, Science and Technology of Japan and from the Nakatani Foundation of Electronic Measuring Technology Advancement.

Address correspondence and reprint requests to Dr. Akihiko Ito, Department of Pathology, Faculty of Medicine, Kinki University, 377-2 Ohno-Higashi, Osaka-Sayama, Osaka 589-8511, Japan. E-mail address: aito@med.kindai.ac.jp

The online version of this article contains supplemental material.

Abbreviations used in this article: Ara-C, cytosine-β-D-arabinofuranoside; BMMC, bone marrow-derived mast cell; CADM1, cell adhesion molecule-1; $[Ca^{2+}]_i$, intracellular Ca^{2+} concentration; DIC, differential interference contrast; DTSSP, 3,3′-dithiobis(sulfosuccinimidyl propionate); E, embryonic day; P, postnatal day; RFP, red fluorescent protein; SCG, superior cervical ganglion; WT, wild-type.

www.jimmunol.org/cgi/doi/10.4049/jimmunol.1002244

both, and this communication was mediated by SCG-derived substance P and its cognate receptor neurokinin-1 expressed on IC-2 cells (25).

CADM1 is a membrane-spanning glycoprotein composed of three extracellular Ig-like domains, a single transmembrane region, and a short carboxyl-terminal intracellular tail with a protein 4.1 interaction sequence and a PDZ type II motif (28–31), and it exerts its function as an adhesion molecule by locating on the cell membrane as a *cis*-dimer (32, 33). As is often the case with Ig superfamily members, CADM1 has several isoforms arising from alternative mRNA splicing, which occurs in the juxtamembranous extracellular region, that is, downstream of the exon encoding the third Ig-like loop and upstream of the exon encoding the transmembrane region (34). In humans and rodents, four membrane-spanning isoforms, CADM1a to d (NCBI accession number of murine CADM1: a, NM_207675; b, NM_207676; c, NM_018770; and d, NM_001025600), are known, which differ in the length of the juxtamembranous extracellular region (34). Mast cells express CADM1c exclusively, whereas brain neurons seem to express various combinations of the four CADM1 isoforms (26, 27, 35). As we will report elsewhere that the binding strength differs considerably among the isoforms that are paired with CADM1c in *trans* interaction (36), CADM1 splicing in neurons may be one of the molecular mechanisms that minutely regulate nerve–mast cell interaction.

In the present study, we examined how the CADM1 splicing pattern changes during the mouse cerebral development and in vitro maturation of hippocampal neurons, and we found that cerebral neurons expressed a developmental stage-specific combination of CADM1a to d. To generate model cells for developing and mature neurons concerning the combination of CADM1 isoforms, Neuro2a mouse neuroblastoma cells that endogenously express CADM1c were modified to additionally express either CADM1b or d, respectively. In cocultures of mast cells on neurite networks of these Neuro2a cells, we examined nerve–mast cell adhesion and communication by loading a femtosecond laser-induced impulsive force on neurite-attendant mast cells and by monitoring intracellular Ca^{2+} concentration ($[Ca^{2+}]_i$) changes in mast cells after adding a nerve stimulant, respectively. These results revealed distinct functions and molecular characters of individual isoforms, and they identified a unique feature of CADM1d, the shortest isoform, that predominates in mature brains.

Materials and Methods

Mice, cells, and Abs

C57BL/6 and ICR mice were purchased from Japan SLC (Hamamatsu, Japan). CADM1 knockout mice were generated and maintained in our laboratory (37). BMMCs from C57BL/6 (BMMCs-wild-type [WT]) and CADM1 knockout mice (BMMCs-CADM1$^{-/-}$) were established as described previously (26, 38). Neuroblastoma cell lines C-1300 and NB-1 were purchased from Riken Bioresource Center (Tsukuba, Japan), and Neuro2a and P19 cells were from the American Type Culture Collection (Rockville, MD). IC-2 cells were maintained as described previously (25). An IC-2 subclone expressing CADM1c was established previously (39). A rabbit polyclonal Ab against the C terminus of CADM1, named RP6, was generated in our laboratory (25). Monoclonal anti–β-actin Ab was purchased from Sigma-Aldrich (St. Louis, MO).

RT-PCR analysis

The procedures for RNA extraction and RT-PCR analyses and details of the primers used were described previously (35).

Western blot analysis

Cells and mouse tissues were lysed in a buffer containing 50 mM Tris-HCl (pH 8.0), 150 mM NaCl, 1% Triton X-100, and protease inhibitor mixture (Sigma-Aldrich). The following procedures were the same as described previously (26, 40). After stripping, the blots were probed with the anti–β-actin Ab.

Plasmid construction and transfection

A mammalian expression vector pCX4-bsr containing the full-length CADM1c cDNA was constructed previously (26). To obtain full-length cDNAs for CADM1b and CADM1d, the following oligonucleotides were synthesized: CADM1b–sense and antisense, 5′-ATACGACACCACGGCGACGACAGAACCAGCAGTTCACGATTC-3′ and 5′-TCGAGAATCGTGAACTGCTGGTTCTGTCGTCGCCGTGGTGTCGT-3′; and CADM1d–sense and antisense, 5′-ATACGATTC-3′ and 5′-TCGAGAATCGT-3′. The sense and antisense oligonucleotides were annealed and inserted into the full-length CADM1c-containing pBluescript vector (26) via the AccI and XhoI sites. The resulting cDNA inserts were excised by EcoRI digestion and inserted directionally into a pCX4-bsr vector via the EcoRI site.

For expression of GFP-tagged CADM1 isoforms, the pEGFP-N1 vector (Clontech Laboratories, Mountain View, CA) was modified to carry an AscI site at the HindIII site of the multiple cloning region, and the pCX4-bsr vectors containing the full-length CADM1 cDNAs were used as templates in PCR together with a pair of primers (5′-GGCGCGCCATGGCGAGTGCTGTGCTGCCGA-3′ and 5′-CCCACCGGTGCGATGAAGTACTCTTTCTTTTCT-3′). The PCR-amplified cDNA fragments were inserted into the modified pEGFP-N1 vector via the AscI and AgeI sites. CADM1d was also expressed as a red fluorescent protein (RFP)-tagged form by using the pDsRed2-N1 vector (Clontech Laboratories). The pCX4-bsr-CADM1d construct was used as a template in PCR together with a pair of primers (5′-ACGCGTCGACGGCAGGTGCCCGACATGGC-3′ and 5′-CCCACCGGTGCGATGAAGTACTCTTTCTTTTCT-3′), and the PCR-amplified cDNA fragment was inserted into the pDsRed2-N1 vector via the SalI and AgeI sites. All the expression vector constructs were confirmed by sequencing to have the expected sequences. The p*Silencer* 3.1-H1 neo vector (Ambion/Applied Biosystems, Foster, CA) was previously modified to express small interfering RNA targeting mouse CADM1 (41).

Using Nucleofector with solution V (Lonza, Basel, Switzerland), Neuro2a cells were transfected in some cases stably with the pCX4-bsr or p*Silencer* 3.1-H1 neo vector constructs, and in other cases transiently with the pCX4-bsr, pEGFP-N1, or pDsRed2-N1 constructs. Stable clones were selected by resistance against blasticidin or G-418 for a month. Transient transfectants were cultured under the conditions described below.

Crosslinking

Neuro2a cells, either intact or transfected with the pCX4-bsr constructs, were cultured for 2 d as described above. The resulting neurite networks were washed twice with PBS and were incubated in PBS containing 2 mM 3,3′-dithiobis(sulfosuccinimidyl propionate) (DTSSP; Pierce, Rockford, IL). After incubation at room temperature for 30 min, Tris-buffered solution (1.0 M) was added to the PBS at a final concentration of 20 mM to stop crosslink reaction, and the cultures were incubated for 15 min. After two rinses with PBS, the cells were lysed in a buffer containing 50 mM Tris-HCl (pH 8.0), 150 mM NaCl, and 1% Triton X-100. The cell lysates obtained were mixed with 4× sample buffer (0.2 M Tris-HCl [pH 6.8], 2% SDS, 20% glycerol, 0.2% bromophenol blue) at a ratio of 3:1 and then boiled at 95°C for 10 min before being subjected to Western blot analyses.

Hippocampal neuron culture

The method for isolation and culture of hippocampal neurons was essentially similar to that described previously (42). Briefly, the hippocampi were isolated from ICR mouse embryos at the age of gestational day 16 and were treated with 0.8% DNase I and 0.5% trypsin (type II-S; Sigma-Aldrich) in HBSS on ice for 13 min. Then, the hippocampal tissues were triturated passing them 10–15 times through a Pasteur pipette and once through a cell strainer (pore size, 70 μm; Falcon; BD Biosciences, Franklin Lakes, NJ). The resulting cell suspension was pelleted down by centrifugation and was resuspended in Eagle's MEM containing 15 mM HEPES, 2% B27 supplement (Life Technologies, Rockville, MD), 5% FCS, and 0.5 mM L-glutamine and then plated onto poly-L-lysine–coated glass-bottomed dishes (MatTek, Ashland, MA). After 2 d, cytosine-β-D-arabinofuranoside (Ara-C), an inhibitor of DNA replication, was added to reach a final concentration of 10 μM. Thereafter, the cultures were left in CO_2 incubator before subjected to RT-PCR or immunofluorescence analyses. The procedure for immunofluorescence was the same as described previously. Briefly, cultured cells were fixed with methanol, incubated with rabbit anti-CADM1 C-terminal peptide Ab, and visualized with Cy2-conjugated anti-rabbit IgG Ab (Jackson ImmunoResearch Laboratories, West Grove, PA).

Establishment of neurite culture and coculture with mast cells

Primary culture of SCG neurons was established following a published protocol (7, 43). Briefly, SCG neurons were plated at a density of 0.5–1.0 × 10^4 neurons/dish onto coverslip-like-bottomed culture dishes of a 35-mm diameter (μ-Dishes; ibidi, Munich, Germany) coated with Matrigel (BD Biosciences) as described previously (35), and they were grown in glial conditioned medium (MB-X9501; Sumitomo Bakelite, Tokyo, Japan) containing 50 ng/ml nerve growth factor (Upstate Biotechnology, Lake Placid, NY) and 5.0 μM Ara-C (Sigma-Aldrich). Neuro2a cells were plated onto Matrigel-coated μ-Dishes at a density of 8.0 × 10^4 cells/dish and were grown in MB-X9501 medium containing 40 ng/ml brain-derived neurotrophic factor (Upstate Biotechnology) and all-*trans* retinoic acid (2.0 μg/ml; Sigma-Aldrich). In some experiments, prior to plating, Neuro-2a cells were transfected with the pEGFP-N1 or pDsRed2-N1 constructs as described above.

After SCG neurons and Neuro2a cells were allowed to extend neurites for 5 and 2 d, respectively, the resulting neurite cultures were washed three times and then overlaid with MB-X9501 medium containing 1.0 × 10^4 BMMCs or IC-2 cells. After 3 h of coculture, the dishes were washed with warmed (37˚C) α-MEM to remove nonadherent BMMCs and IC-2 cells and were then subjected to femtosecond laser irradiation assays. To examine nerve–mast cell communication, Neuro2a-IC-2 cell cocultures were continued for 2 d in the presence of IL-3 (3 ng/ml). In some experiments, Neuro2a neurite cultures were labeled with FM4-64 styryl dye (Molecular Probes, Eugene, OR) according to the manufacturer's instructions. FM dyes are taken up into, and released from, active nerve terminals in response to synaptic stimulation, and thus they allow direct visualization of synaptic boutons at nerve endings and bouton-like punctate structures dotting along neurites, both of which are active in exo- and endocytosis of synaptic vesicles (44). Briefly, FM4-64 solution (solvent, water) was added to the neurite cultures at a concentration of 5 μg/ml. After 20 min incubation at 37˚C in 5% CO_2, the cultures were gently washed with warmed (37˚C) α-MEM and then filled with MB-X9501 medium. Fluorescent images of live cells were captured through a confocal laser scanning microscope (A1; Nikon, Tokyo, Japan) equipped with a CO_2 chamber unit for cell culture.

Femtosecond laser irradiation assay

An inverted microscope (IX71; Olympus, Tokyo, Japan) was equipped with a CO_2 chamber unit for cell culture, a CCD camera with a video recorder, and a laser beam path from a femtosecond laser generator. This apparatus is our original, and it was described in detail elsewhere (36). In the present study, nerve–mast cell adhesion was quantified using this apparatus as follows. Nerve–mast cell cocultures were established in μ-Dishes and placed in the CO_2 chamber unit on an electric stage of the microscope. First, we focused femtosecond laser shots at a position a few 10 μm apart from neurite-attendant BMMCs-WT and adjusted the laser pulse energy so that single laser shots resulted in detachment of some BMMCs-WT but not others. Next, we repeated laser shots at the adjusted pulse energy as follows (see Supplemental Fig. 1). The focal point of the first shot was positioned 100 μm far from a mast cell to be targeted, and the second shot was focused ~5–10 μm nearer the target. The following shots were repeated in a similar manner until the mast cell detached. All the processes were video recorded, and the distance between the last shot focal point and the target mast cell ($L_{max\ to\ detach}$) was measured. Approximately 100 mast cells were selected randomly as a target and were individually examined for their $L_{max\ to\ detach}$.

Cellular activation and $[Ca^{2+}]_i$ measurement

As described previously, the calcium fluorophore Fluo-8-AM (ABD Bioquest, Sunnyvale, CA) was used to assess Ca^{2+} mobilization as an indicator (25, 41). Briefly, after 2-d-long coculture of nerve and mast cells, both cells were incubated in culture medium containing 1 μM Fluo-8-AM for 30 min, followed by three rinses in HEPES buffer (10 mM HEPES [pH 7.2], 140 mM NaCl, 5 mM KCl, 0.6 mM $MgCl_2$, 1 mM $CaCl_2$, 0.1% glucose, 0.1% BSA, and 0.01% sulfinpyrazone). The coculture dishes were filled with HEPES buffer and placed in a CO_2 chamber unit on a stage of a confocal laser scanning microscope (LSM510; Carl Zeiss, OberKochen, Germany). Fluorescent images for Fluo-8 were taken every 5 s using excitation and emission wavelengths of 488 and >505 nm, respectively. Differential interference contrast (DIC) images were also taken. At 15 s after the initiation of image capture, histamine (Sigma-Aldrich; stock solution, 10 mM in HEPES buffer) was added to the dishes at a concentration of 1 mM. Captured fluorescence images were analyzed with the Scenic Pro M7 computer analysis system (Siemens, Munich, Germany) as described previously. Neurite-attendant mast cells were considered to be responding to Neuro2a cell activation when they met the following four conditions: 1) Fluo-8 fluorescence intensity increased in Neuro2a cells immediately after the histamine addition (within <10 s); 2) subsequently, fluorescence intensity increased in neurite-attendant mast cells by >25 arbitrary units (>50% of the baseline); 3) there was a 10 s or longer time lag between the two onsets of the intensity increases; and 4) the intensity increase in Neuro2a cells lasts >20 s. At least 12 coculture dishes were prepared per experimental group, and data were obtained from >50 neurite–mast cell units. All results were reproduced twice by independent experiments.

Behavior of cytoplasmic granules

Because cytoplasmic granules of mast cells contain histamine and serotonin abundantly, they are easily stained with a weakly basic, cell-permeable fluorescence compound, quinacrine (45). As described above, Neuro2a and IC-2 cells were cocultured for 2 d and incubated in culture medium containing 3 μM quinacrine dihydrochloride (Wako Pure Chemicals, Osaka, Japan) for 15 min. The dishes were washed with HEPES buffer three times and then filled with the buffer. The cocultures were added with histamine or solvent (HEPES buffer) and were observed using LSM510 as described above. Multiple cytoplasmic granules of IC-2 cells were visualized by green fluorescence. After the histamine addition, some of the granules became undetectable. When >10% of cytoplasmic granules contained in one IC-2 cell became undetectable within 3 min after the addition of histamine of solvent, we judged that "disappearance of mast cell granules after nerve activation" occurred in the IC-2 cell.

Statistical analysis

The Student *t* test was performed for analyzing $L_{max\ to\ detach}$, and the χ^2 test was performed for analyzing the proportions of responders using the StatView software (Abacus Concepts, Cary, NC) on a Macintosh computer. A *p* value <0.01 was considered to be significant. Details of the regression analysis of $L_{max\ to\ detach}$ are described in Supplemental Table I.

Results

Developmental regulation of CADM1 isoform splicing in cerebral neurons

We designed a pair of PCR primers so as to encompass the CADM1 extracellular juxtamembrane region, in which alternative splicing occurs, and examined the CADM1 mRNA expression in the mouse cerebrum at various ages by RT-PCR analyses using the primers (Fig. 1*A*). The PCR products were detected as multiple ladders on agarose gels (Fig. 1*B*). When compared with molecular size markers for known isoforms, the cerebrum was found to contain four transcripts encoding CADM1 isoforms (a–d), and the individual transcripts appeared to be quantitatively regulated in a developmental stage-specific manner. It was noticeable that the CADM1 splicing pattern drastically changed between postnatal day (P) 7 and 14; before P14, the major isoforms were CADM1b and CADM1c, but after P14, it switched to CADM1d, which was nearly undetectable before P14. CADM1a was detected at all examined time points, and its expression level was relatively low and constant. Mouse hippocampal neurons were isolated from a fetal brain at embryonic day (E) 16 and were cultured for 2 wk in the presence of neuron culture supplements. Neurite networks emerged in a week and grew increasingly more elaborate through the next week (Supplemental Fig. 2). RT-PCR analyses revealed that the cultured hippocampal neurons expressed four CADM1 isoforms (a–d) and their splicing pattern drastically changed during the culture period in a similar fashion as observed in mouse cerebrums aged from E18 through P14 (Fig. 1*C*). Here again, CADM1d was not detectable until elaborate neurite networks emerged in the culture.

Different patterns of distribution and dimerization of individual CADM1 isoforms on Neuro2a neurites

We screened for CADM1 mRNA expression in several neuronal cell lines, including Neuro2a neuroblastoma cells, and found that all examined cells had one main CADM1 isoform and that Neuro-

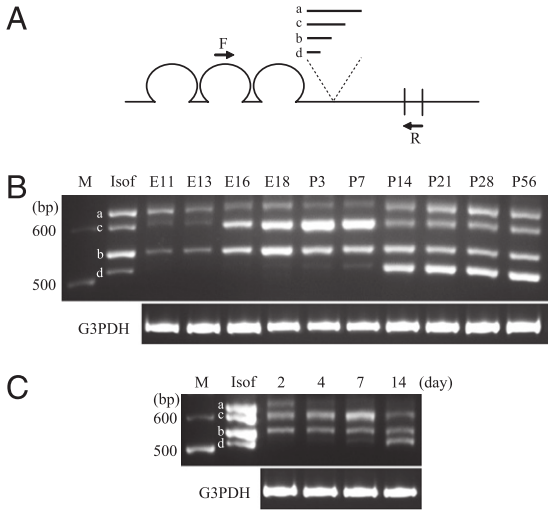

FIGURE 1. Changes in the expression of CADM1 isoforms during the mouse brain development and hippocampal neurite network formation. As illustrated in *A*, a set of forward (F) and reverse (R) primers was designed so as to encompass the alternative splice region. Total RNAs were extracted from mouse cerebrums at various ages (*B*) and E16 hippocampal neurons cultured for indicated days (*C*), and they were amplified by RT-PCR using the primer set, and then the products were electrophoresed on 3% agarose gels. Equal input of total RNA per lane was verified by amplification of G3PDH mRNA. Isof, cDNA fragments for CADM1 isoforms (a–d); M, 100-bp ladder size marker.

2a cells expressed CADM1c exclusively (Supplemental Fig. 3). Using Neuro2a cells, we examined how individual CADM1 isoforms were distributed on neurites. Neuro2a cells were transiently transfected with the plasmid vector expressing CADM1b, CADM1c, or CADM1d that was fused with GFP at its C terminus (CADM1b-GFP, CADM1c-GFP, or CADM1d-GFP) and were observed under an epifluorescence microscope. As shown in Fig. 2*A*, CADM1b-GFP and CADM1c-GFP were distributed nearly homogeneously along Neuro2a neurites, whereas CADM1d-GFP showed a punctate distribution. When neuritic regions with synaptic activity were visualized by short-term application of FM4-64 styryl dye, CADM1d appeared to accumulate sometimes in bouton-like punctate structures, some of which were recognized structurally as neuritic varicosities (Fig. 2*A*, arrowheads).

Non–GFP-tagged forms of CADM1b and CADM1d were transiently expressed in Neuro2a cells and were treated with or without a NHS-ester crosslinker, DTSSP. Cell lysates were prepared from the transfectants and original Neuro2a cells and were subjected to Western blot analyses using a CADM1 Ab. Crosslinking treatment resulted in emergence of multiple bands ranging in electrophoretic mobility from 135 to 185 kDa, which were considered CADM1 isoform dimers because the band sizes were nearly double those of the isoform monomers (Fig. 2*B*). Judging from the mobility size, when either CADM1b or CADM1d was coexpressed with CADM1c in Nuero2a cells, each of the isoforms appeared to form *cis*-homodimers exclusively, except that small amounts of *cis*-heterodimers were formed between CADM1c and CADM1d. These results suggested that CADM1d clustered along Neuro2a neurites, and each of the clustering foci consisted of an assembly of CADM1d *cis*-homodimers.

Different contributions of individual CADM1 isoforms to nerve–mast cell adhesion: quantification by femtosecond laser

Developmentally regulated changes in the expression of CADM1 isoforms in nerves may influence nerve–mast cell adhesion. We considered that a femtosecond laser could be a powerful tool to

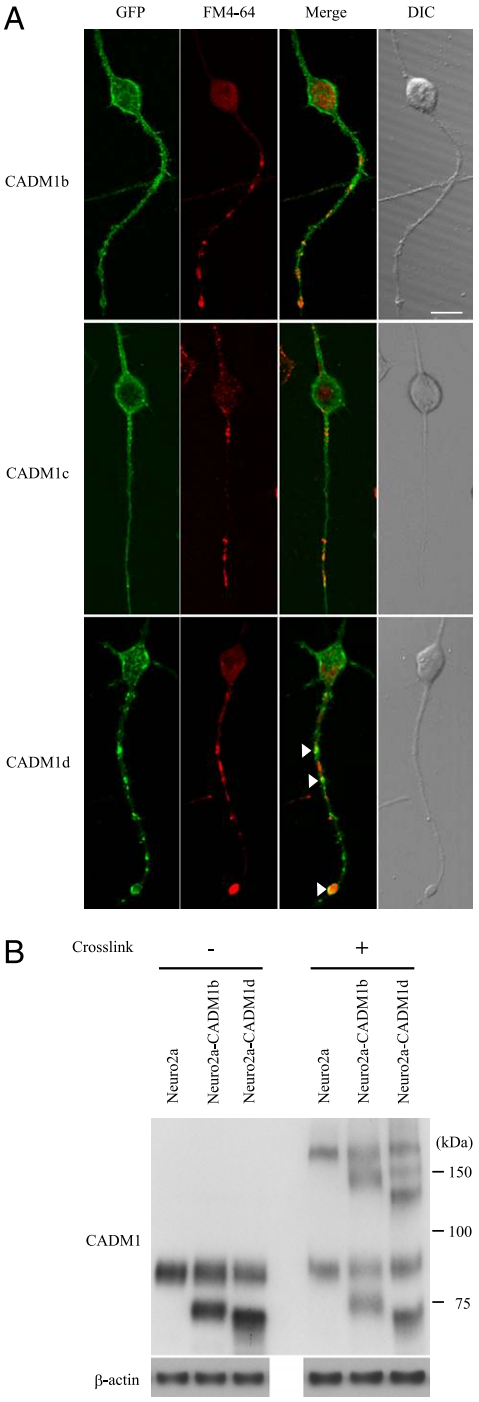

FIGURE 2. Distinct patterns of localization and dimerization of individual CADM1 isoforms on Neuro2a neurites. *A*, Subcellular localization of CADM1 isoforms on Neuro2a neurites. Neuro2a cells were transiently transfected with the plasmid vector expressing CADM1b-GFP, CADM1c-GFP, or CADM1d-GFP and were loaded with FM4-64 to visualize bouton-like punctate structures. Note that CADM1d-GFP signals cluster along neurites and some of the clustering foci are colocalized with FM4-64 signals (arrowheads). Scale bar, 10 μm. *B*, Crosslinking experiments of CADM1b and CADM1d coexpressed with CADM1c in Neuro2a cells. Neuro2a cells were transiently transfected with pCX4-bsr vector expressing CADM1b or CADM1d and were then treated with (+) or without (−) DTSSP crosslinker. Cell lysates were prepared from Neuro2a cells treated as indicated, electrophoresed on a 7.5% polyacrylamide gel, and blotted with anti-CADM1 Ab. After stripping, the blot was reprobed with anti–β-actin Ab to indicate the protein loading per lane.

estimate the adhesive strength of individual mast cells attached to neurites, because this laser can induce impulsive force that propagates from its focal point and reaches as far as 100 μm when it is focused in aqueous solution (36, 46, 47). To examine this idea, we cocultured BMMCs-WT on neurite networks sprouting out from SCG neurons and focused femtosecond laser shots approximately a few 10 μm apart from neurite-attendant BMMCs-WT. When the single laser shot energy was 850 nJ/pulse, some mast cells were detached from neurites with leaving the neurites as they were, but other mast cells were not (Fig. 3*A*). To estimate the adhesive strength of individual BMMCs-WT to SCG neurites, we repeatedly focused the laser shots with this energy in the vicinity of target BMMCs-WT as described in Supplemental Fig. 1, and we measured the distance between the last laser focal point and the target ($L_{max\ to\ detach}$). We examined 100 BMMCs-WT selected randomly as a target and displayed a histogram of $L_{max\ to\ detach}$ in Fig. 3*B*. Similar experiments were performed in the coculture of SCG neurons and BMMCs-CADM1$^{-/-}$ (Fig. 3*C*). The mean $L_{max\ to\ detach}$ of BMMCs-CADM1$^{-/-}$ was significantly larger than that of BMMCs-WT ($p < 0.0001$). According to our original method for impulsive force estimation (36), the two $L_{max\ to\ detach}$ histograms were converted to histograms given by a function of impulse (Newton × time) (Supplemental Fig. 1). These results not only reconfirmed the pivotal role for CADM1 in nerve–mast cell adhesion, but also indicated the usefulness of femtosecond laser irradiation to quantify the nerve–mast cell adhesion.

Instead of SCG neurons, Neuro2a cells were cocultured with BMMCs. Neuro2a cells were allowed to extend neurites for 2 d in glial conditioned medium containing brain-derived neurotrophic factor, and BMMCs-WT or BMMCs-CADM1$^{-/-}$ were plated onto the neurite networks. After 5 h coculture, Neuro2a-BMMC adhesion strength was quantified by femtosecond laser irradiation. Here again, the mean $L_{max\ to\ detach}$ of BMMCs-CADM1$^{-/-}$ was significantly larger than that of BMMCs-WT ($p < 0.0001$) (Fig. 3*D*, 3*E*). In an attempt to generate model cells for cerebral neurons either developing (before P14) or mature (after P14), we modified Neuro2a cells to express additionally either CADM1b (Neuro2a-CADM1b) or CADM1d (Neuro2a-CADM1d), respectively. Western blot analyses of CADM1 in these sublines revealed a slight reduction in the endogenous expression level of CADM1c, suggesting possible mechanisms by which the total amount of CADM1 isoforms expressed per cell is controlled not to be excessive (Fig. 4*A*). When we established neurite networks from original Neuro2a cells and the two subclones, there was no considerable difference in the degree of neurite extension among the three types of cells (data not shown). Cocultures of the two sublines and BMMCs-WT were subjected to femtosecond laser irradiation assays. As shown in Fig. 4*B–D*, the means of $L_{max\ to\ detach}$ in the cocultures with Neuro2a-CADM1b and Neuro2a-CADM1d cells were significantly smaller than the mean in the coculture with original Neuro2a cells, indicating that additional expression of either CADM1b or CADM1d resulted in reinforcement of BMMCs-WT adhesion to Neuro2a neurites. Interestingly, when we approximated the $L_{max\ to\ detach}$ histograms to a Gaussian distribution, we found that the histogram of the Neuro2a-CADM1d coculture could be divided into two Gaussian curves, one with a median of 10.9 μm and the other 21.2 μm (Fig. 4*D*, dotted lines). Notably, the median value of the former curve was markedly smaller than the means in the cocultures with original Neuro2a and Neuro2a-CADM1b cells. We knocked down endogenous CADM1c in Neuro2a-CADM1d cells (Supplemental Fig. 4) and cocultured the resultant cells that expressed CADM1c a little and CADM1d abundantly with BMMCs-WT. The $L_{max\ to\ detach}$ histogram of this coculture was also bimodal, but the Gaussian curve with a smaller median apparently dominated over the other with a larger median (Fig. 4*E*). Additionally, we prepared two types of cocultures: 1) Neuro2a cells with CADM1c knocked down and BMMCs-WT, and 2) Neuro2a-CADM1d cells with BMMCs-CADM1$^{-/-}$. The $L_{max\ to\ detach}$ histograms of both cocultures were unimodal, and the medians were equivalent to those of Neuro2a-BMMCs-CADM1$^{-/-}$ cocultures (Supplemental Fig. 4). These

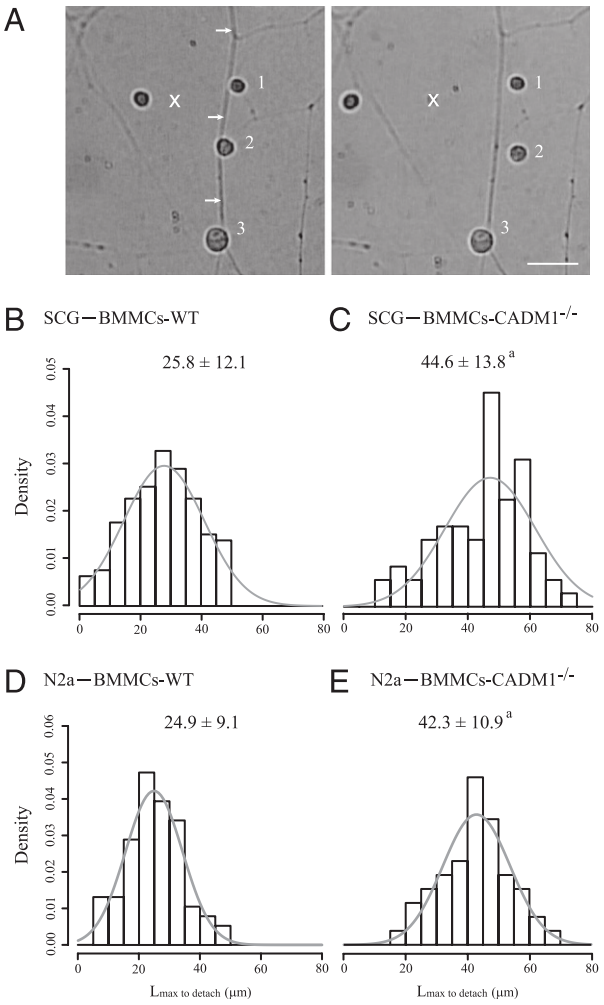

FIGURE 3. Estimation of the adhesive strengths of individual BMMCs attaching to SCG neurites by femtosecond laser irradiation. *A*, BMMCs-WT were cocultured on SCG neuron neurite networks for 5 h, and a single femtosecond laser shot (850 nJ/pulse) was focused at a position ~50 μm apart from neurite-attendant BMMCs. Example photomicrographs are shown that are selected from video images recorded before and after laser irradiation. Before irradiation (*left*), three BMMCs-WT (numbered 1, 2, and 3) are observed attaching to a SCG neurite (indicated by arrows). Immediately after irradiation (*right*), BMMCs-WT nos. 1 and 2 are detached from the neurite, while BMMC-WT no. 3 remains attendant. Note that the former BMMCs are positioned nearer to the laser focal point (depicted by ×) than the latter. Scale bar, 20 μm. *B* and *C*, BMMCs-WT (*B*) or BMMCs-CADM1$^{-/-}$ (*C*) were cocultured on SCG neuron neurite networks, and $L_{max\ to\ detach}$ was measured for individual BMMCs. After a neurite-attendant BMMC was randomly selected as a target, femtosecond laser shots were repeated as their focal points were made getting gradually closer to the target BMMC until the target was detached from the neurite. $L_{max\ to\ detach}$ was measured for ~100 BMMCs in each group and was expressed as a histogram (*B*, *C*). The mean and SD (μm) were shown above the histogram. According to the least squares method, probability density distribution of $L_{max\ to\ detach}$ was approximated to a Gaussian curve (gray). [a]$p < 0.0001$ by *t* test when compared with the value of BMMCs-WT.

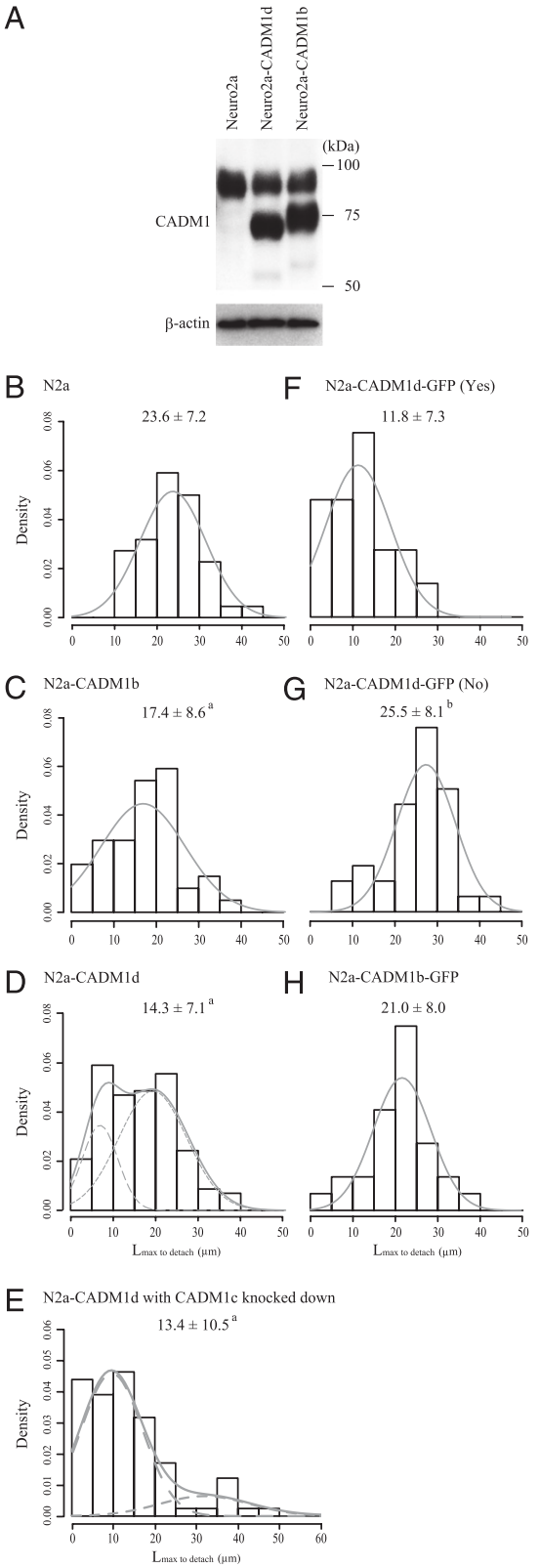

FIGURE 4. Differential effects of CADM1b and CADM1d on BMMC adhesion to Neuro2a neurites. *A*, Western blot analyses of CADM1 in original Neuro2a and its two subclones, Neuro2a-CADM1b and Neuro2a-CADM1d. Cell lysates were electrophoresed on a 10% SDS-PAGE gel and were blotted with anti-CADM1 Ab. After stripping, the blot was reprobed with anti–β-actin Ab to indicate the protein loading per lane. *B–H*, Histograms of $L_{max\ to\ detach}$ of BMMCs-WT in various cocultures. BMMCs-WT were cocultured with Neuro2a (*B*, *F–H*), Neuro2a-CADM1b (*C*), Neuro2a-CADM1d (*D*), or Neuro2a-CADM1d cells with CADM1c knocked down (*E*). In *F–H*, prior to the initiation of coculture, Neuro2a cells were transiently transfected with the plasmid vector expressing either CADM1d-GFP (*F*, *G*) or CADM1b-GFP (*H*), and in *F* and *G*, neurite-attendant BMMCs-WT were divided into two groups; those present on the CADM1d assembly site (*F*) and those present elsewhere (*G*). $L_{max\ to\ detach}$ was measured for ~100 BMMCs in each of the coculture groups, and it was expressed as a histogram. The mean and SD (μm) were shown above the histogram. According to the least squares method, probability density distribution of $L_{max\ to\ detach}$ was approximated to one Gaussian curve (gray solid line), except for *D* and *E*, where two Gaussian curves were deduced (gray dotted lines) and were merged into one (bimodal line). [a]$p < 0.0001$ by *t* test when compared with the values of *B*; [b]$p < 0.0001$ by *t* test when compared with the values of *F*.

results suggested that CADM1d had a much larger potential to strengthen BMMCs-WT adhesion to Neuro2a neurites than CADM1b.

Enhanced nerve–mast cell adhesion and communication at the CADM1d assembly site on Neuro2a neurites

We speculated that the bimodality of the mast cell adhesion strength to Neuro2a-CADM1d neurites might be attributable to CADM1d clustering along neurites. To visualize the CADM1d assembly on neurites, Neuro2a cells were transiently transfected with cDNA encoding CADM1d-GFP, and they were allowed to sprout out neurites. After 2 d, BMMCs-WT were cocultured on the neurite networks for 5 h and were then estimated for their adhesive strengths by the femtosecond laser assay. In this assay, neurite-attendant BMMCs-WT were divided into two groups: those present on the CADM1d assembly site and those present elsewhere. As summarized by histograms in Fig. 4*F* and 4*G*, the former and latter groups had significantly different means of $L_{max\ to\ detach}$, that is, 11.8 ± 7.3 and 25.5 ± 8.1 μm, respectively. The latter mean was nearly double the former. Notably, a similar relationship was seen between the two medians (10.9 and 21.2 μm) of the two Gaussian curves, into which the bimodal $L_{max\ to\ detach}$ histogram of the Neuro2a-CADM1d coculture was divided by approximation (compare Fig. 4*D*, 4*F*, and 4*G*). As shown by comparison between the two histograms of Neuro2a-CADM1b and Neuro2a-CADM1b-GFP cocultures (Fig. 4*C*, 4*H*), GFP-tagging to CADM1 isoforms seemed to result in ~20% larger $L_{max\ to\ detach}$. These results suggested that CADM1d clustering foci on Neuro2a-CADM1d neurites mediated significantly firmer adhesion of BMMCs-WT to the neurites than elsewhere.

Next, we examined how CADM1 isoforms on Neuro2a cells influence nerve–mast cell communication. For this purpose, we used IC-2 cells, a BMMC-derived mast cell line that lacks endogenous CADM1, but not BMMCs-WT, because BMMCs-WT are known to respond poorly to nerve activation, probably due to their low expression level of neurokin-1 receptor at the steady-state (12, 23). We previously cocultured IC-2 cells that expressed CADM1c exogenously (IC-2^{CADM1c}) or not with SCG neurons, and we showed that exogenous CADM1c markedly enhanced the responsiveness of IC-2 cells to SCG neuron activation (48). In the present study, we cocultured IC-2^{CADM1c} cells on neurite networks extending from various types of Neuro2a cells and used histamine to activate Neuro2a cells specifically, because histamine induced Ca^{2+} mobilization in Neuro2a cells, but not IC-2^{CADM1c} cells apart from neurites, when it was added to the coculture at a concentration of 1 mM (data not shown). First, we plated IC-2^{CADM1c} cells onto neurite cultures of original Neuro2a and Neuro2a-CADM1b and Neuro2a-CADM1d cells and cocultured them for 2 d. After all of the cultured cells were loaded with the Ca^{2+} indicator Fluo-8, we added histamine to the coculture at a concentration of 1 mM

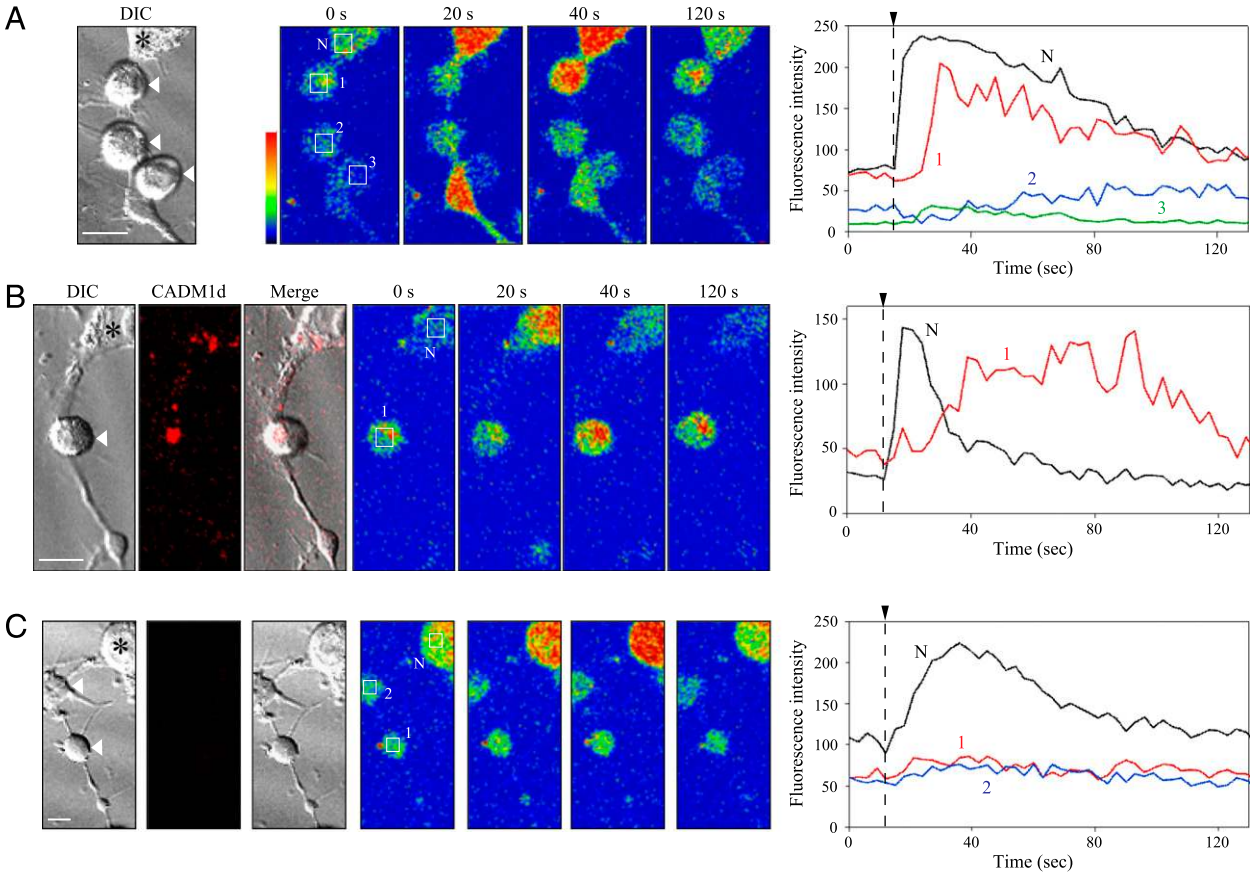

FIGURE 5. $[Ca^{2+}]_i$ changes in IC-2^{CADM1c} cells attaching to Neuro2a neurites after specific activation of Neuro2a cells. *A–C*, Neuro2a and IC-2^{CADM1c} cells were cocultured for 2 d and were then loaded with Fluo-8. In *B* and *C*, prior to the initiation of coculture, Neuro2a cells were transiently transfected with the plasmid vector expressing CADM1d-RFP. After Fluo-8 fluorescence detection was started in a 5-s interval, histamine was added to the coculture at a concentration of 1 mM. Representative DIC and Fluo-8 fluorescence (green) images at the indicated time points are shown in panels. In *B* and *C*, RFP fluorescence (red) images were also captured (CADM1d) and merged with DIC (merge). *B* and *C* show representative results of IC-2^{CADM1c} cells present on CADM1d assembly and those present elsewhere, respectively. In the $t = 0$ panels, several regions of interest (boxed by white lines) are defined in a Neuro2a cell (N) and some IC-2^{CADM1c} cells (1, 2, and 3). The fluorescence intensity is displayed in pseudo color, with blue indicating the least fluorescence: the scale bar is shown at the left of the $t = 0$ panel in *A*. Traces of fluorescence intensity for each region of interest are shown as line graphs, and the time points of histamine addition are indicated by dotted lines with arrowheads (*right panels*). Asterisks and arrowheads in DIC images depict cell bodies of Neuro2a cells and IC-2^{CADM1c} cells, respectively. Scale bars, 10 μm.

and then monitored the changes in $[Ca^{2+}]_i$ in three types of Neuro2a cells and IC-2^{CADM1c} cells by tracing fluo-8 fluorescence. A representative result from the coculture with original Neuro2a cells is shown in Fig. 5*A*; $[Ca^{2+}]_i$ increased in Neuro2a cell bodies and neurites immediately after the histamine addition, and after a 10 s or longer time lag following the onset of Neuro2a cell activation, $[Ca^{2+}]_i$ increased in some proportion of neurite-attendant IC-2^{CADM1c} cells with a duration time >1 min. When we regarded IC-2^{CADM1c} cells with >50% increase from baseline in $[Ca^{2+}]_i$ as responders to nerve activation, we found that the proportion of IC-2^{CADM1c} responders was significantly higher in Neuro2a-CADM1d coculture than in original Neuro2a and Neuro2a-CADM1b cocultures (Table I). Next, Neuro2a cells were transiently transfected with cDNA encoding RFP-tagged CADM1d (Neuro2a-CADM1d-RFP) and were allowed to sprout out neurites for 2 d, then cocultured with IC-2^{CADM1c} cells for 2 d. By visualizing RFP signals, we divided IC-2^{CADM1c} cells that were attendant to RFP signal-positive neurites into two groups: those present on the CADM1d assembly and those present elsewhere (Fig. 5*B*, 5*C*). The proportion of IC-2^{CADM1c} responders was significantly higher in the former group (Table I). Considering that the proportion in Neuro2a-CADM1d-RFP coculture was somewhat lower than that in Neuro2a-CADM1d coculture, RFP-tagging to CADM1d may result in impaired function of CADM1d. Because CADM1d appeared to sometimes accumulate in neuritic varicosities that are labeled with FM4-64 dye (Fig. 2*A*), it was suggested that nerve–mast cell interaction might be enhanced at bouton-like punctate structures independently of CADM1d. To examine this possibility, we cocultured IC-2^{CADM1c} cells on Neuro2a neurites that were labeled with FM4-64 dye and divided

Table I. Responsiveness of IC-2^{CADM1c} cells to Neuro2a cell activation in cocultures of both cells

Type of Neuro2a Cells[a]	Red Fluorescence Accumulation at IC-2^{CADM1c} Cell Adhesion Site	No. of IC-2^{CADM1c} Cells		*p* Value
		Total	Responder	
Neuro2a		87	35	
Neuro2a-CADM1b		89	36	0.98[b]
Neuro2a-CADM1d		113	75	<0.001[b]
Neuro2a-CADM1d-RFP	Yes	126	79	0.0040
	No	47	18	
Neuro2a, FM4-64 labeled	Yes	30	11	0.87
	No	26	9	

[a]Used for coculture with IC-2^{CADM1c} cells.
[b]By χ^2 test when compared with the value of the Neuro2a coculture.

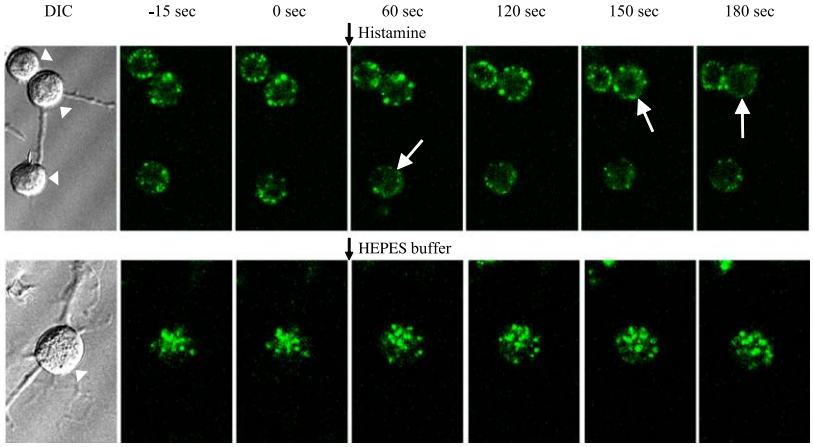

FIGURE 6. Behavior of cytoplasmic granules of IC-2^{CADM1c} cells attaching to Neuro2a neurites after specific activation of Neuro2a cells. Neuro2a and IC-2^{CADM1c} cells were cocultured for 2 d and were then loaded with quinacrine. After quinacrine, fluorescence detection was started in a 5-s interval, histamine was added to the coculture at a concentration of 1 mM (*upper*), or solvent alone (HEPES buffer) was added (*lower*). Representative DIC and quinacrine fluorescence (green) images at the indicated time points are shown in panels. Arrowheads in DIC images depict IC-2^{CADM1c} cells attaching to neurites. Arrows in green fluorescence images depict IC-2^{CADM1c} cells in which >10% cytoplasmic granules disappeared when compared with the images taken before 30 or 60 s. Original magnification ×200.

neurite-attendant IC-2^{CADM1c} cells into two groups: IC-2^{CADM1c} cells present on FM4-64–labeled sites and those present elsewhere. The proportions of IC-2^{CADM1c} responders to neurite activation were comparable between the two groups (Table I). These results collectively suggested that the responsiveness of neurite-attendant IC-2^{CADM1c} cells to nerve activation was enhanced specifically at CADM1d assembly sites.

To access the functional relevance of $[Ca^{2+}]_i$ increase in IC-2^{CADM1c} responders, we observed the behavior of cytoplasmic granules of IC-2^{CADM1c} cells after Neuro2a activation. We loaded Neuro2a-IC-2^{CADM1c} cell cocultures with quinacrine and visualized multiple cytoplasmic granules of IC-2^{CADM1c} cells by green fluorescence. Some of the granules disappeared in 3 min, when histamine, but not solvent alone, was added to the cocultures (Fig. 6). This event of granule disappearance following histamine addition was observed more often in IC-2^{CADM1c} cells when they were cocultured with Neuro2a-CADM1d cells than with original Neuro2a cells (Table II). Neuronal CADM1d not only strengthened nerve–mast cell adhesion, but appeared also to promote mast cell degranulation following nerve activation.

Discussion

In the present study, we showed that four CADM1 isoforms (a–d) were expressed in the mouse cerebrum, and their combination and expression level dramatically changed as the cerebrum grew mature. Interestingly, when E16 hippocampal neurons were grown in vitro for 2 wk, they performed RNA splicing on CADM1 transcripts in a fashion similar to the cerebrum from E18 to P14. These results suggested that individual neurons expressed multiple CADM1 isoforms, and the isoform splicing pattern was critically regulated at the single neuron level and in a developmental stage-dependent manner, because 1) cerebral neurons are thought principally not to proliferate after birth (49), 2) cell proliferation was inhibited in the hippocampal neuron culture by Ara-C treatment, and 3) CADM1 is reported to be expressed exclusively by neurons but not glial cells (50, 51). We found that the splicing pattern of CADM1 isoforms drastically changed in the cerebrum between P7 and P14. Because the postnatal second week is known as the period when neuronal networks develop progressively in the cerebrum (52), CADM1 isoforms are suggested to have individually specific roles in the network formation. What splicing factors may regulate the CADM1 splicing event and how the CADM1 splicing event may be involved in neuronal network elaboration are now under investigation in our laboratory.

We focused on the finding that developing cerebral neurons expressed mainly CADM1b and CADM1c, and that the mature neurons expressed CADM1d additionally and predominantly, and therefore we compared Neuro2a-CADM1b and Neuro2a-CADM1d cells in the coculture with mast cells. Currently, we established a noncontact measurement system for intercellular adhesion strength assisted by femtosecond laser (36). By applying this system to nerve–mast cell coculture, we successfully estimated the adhesive strength of individual mast cells to neurites, and we found that BMMCs-WT adhered to Neuro2a-CADM1d neurites significantly firmer than to Neuro2a-CADM1b neurites. To address molecular bases for this phenomenon, we coupled the femtosecond laser assay with GFP-tagging and crosslinking experiments and revealed that CADM1d clustered along Neuro2a neurites, and that each of the clustering foci consisted of an assembly of CADM1d homodimers and served as a firmer adhesion site for BMMCs-WT. This ability of CADM1d to strengthen nerve–mast cell adhesion was likely to result simply from its dense accumulation at the mast cell contact sites, because 1) BMMCs-WT expressed CADM1c exclusively (26, 27), and 2) heterotypic cell aggregation and femtosecond laser irradiation assays consistently showed that CADM1c-CADM1b and CADM1c-CADM1d bindings in *trans* had comparable adhesion strength. Interestingly, Ca^{2+} imaging experiments revealed that the CADM1d clustering foci along Neuro2a neurites served for mast cells as not only a firmer adhesion site but also a more efficient communication site. This site may be of functional relevance, because mast cell degranulation appeared to be promoted when nerve–mast cell contact occurred via this site. In contrast to CADM1d, CADM1b did not enhance the efficacy of Neuro2a-BMMC communication when expressed in Neuro2a cells, although it significantly strengthens the adhesion between both. Because CADM1d predominates over CADM1b in mature cerebral neurons and the reverse is true of developing neurons, nerve–

Table II. Behavior of quinacrine-labeled cytoplasmic granules of IC-2^{CADM1c} cells after specific activation of Neuro2a cells in cocultures of both cells

Type of Neuro2a Cells[a]	Disappearance of IC-2^{CADM1c} Cell Granules after Neuro2a Cell Activation[b]		p Value[c]
	Yes	No	
Neuro2a	7	37	0.046
Neuro2a-CADM1d	13	24	

[a]Used for coculture with IC-2^{CADM1c} cells (see Fig. 6).
[b]Whether granule disappearance occurred (Yes) or not (No) was judged according to the criteria described in *Materials and Methods*.
[c]By χ^2 test.

mast cell interaction is supposed to be reinforced in mature brains, when compared with developing brains.

Structurally, CADM1d differs from the other three (a–c) isoforms; that is, in the extracellular juxtamembrane region, the isoforms other than CADM1d have *O*-glycans probably linked to the threonine residues, whereas CADM1d does not have such structures (34). The presence or absence of *O*-glycans may be involved in determining the accessibility of association partner molecules to each isoform. In fact, it is reported that CADM1a and CADM1b, but not CADM1d, are processed by TACE/ADAM17-like proteases in the extracellular juxtamembrane region (53). Such membrane-type metalloproteases are supposed to be associated with CADM1a and CADM1b in their neighborhood, but not with CADM1d. Although the amino acid sequence of the intracellular domain is identical among the four isoforms, CADM1d may have particular association partners different from those of the other isoforms, due to the lack of *O*-glycans. A series of our past studies has consistently shown that nerve-to-mast cell communication should be mediated by substance P and its receptor neurokinin-1 (25). Although future studies should reveal what determines CADM1d localization along neurites and its preference for synaptic bouton-like structures, CADM1d clustering at particular neuritic foci may trigger assemblage of machinery necessary for efficient release of substance P from each focus.

It has long been known that mast cells are resident in the brain, primarily in thalamic and hippocampal regions (54, 55), but the function of mast cells in the brain remains controversial. Currently, Nautiyal et al. (56) demonstrated that brain mast cells are implicated in the modulation of anxiety-like behavior and provided evidence for the behavioral importance of neuroimmune links by using mast cell-deficient $Kit^{W\text{-}sh/W\text{-}sh}$ mice. CADM1 may be implicated in such neuroimmune links by directly mediating nerve–mast cell interaction, and CADM1 splicing switch in cerebral neurons can be one of the critical molecular mechanisms that underlie behavioral modulation, as suggested by the present study. In the peripheral tissues, nerve–mast cell interaction is regarded as a key element of neurogenic inflammation, which is involved in the pathophysiology of various diseases, such as irritable bowel syndrome and contact hypersensitivity (20, 21, 57). Although peripheral nerves, such as SCG and dorsal root ganglia, appear to express CADM1c exclusively under physiologic conditions (25) (Supplemental Fig. 3), there may be some pathological conditions in which the CADM1 splicing pattern changes in peripheral nerves, and as a result, nerve–mast cell interaction is reinforced, causing exacerbation of neurogenic inflammation.

Disclosures

The authors have no financial conflicts of interest.

References

1. Kitamura, Y., M. Shimada, K. Hatanaka, and Y. Miyano. 1977. Development of mast cells from grafted bone marrow cells in irradiated mice. *Nature* 268: 442–443.
2. Nakahata, T., and M. Ogawa. 1982. Identification in culture of a class of hemopoietic colony-forming units with extensive capability to self-renew and generate multipotential hemopoietic colonies. *Proc. Natl. Acad. Sci. USA* 79: 3843–3847.
3. Austen, K. F., and J. A. Boyce. 2001. Mast cell lineage development and phenotypic regulation. *Leuk. Res.* 25: 511–518.
4. Khalil, M., J. Ronda, M. Weintraub, K. Jain, R. Silver, and A. J. Silverman. 2007. Brain mast cell relationship to neurovasculature during development. *Brain Res.* 1171: 18–29.
5. Selye, H. 1965. *The Mast Cells.* Butterworths, Washington, D.C.
6. Stead, R. H., M. F. Dixon, N. H. Bramwell, R. H. Riddell, and J. Bienenstock. 1989. Mast cells are closely apposed to nerves in the human gastrointestinal mucosa. *Gastroenterology* 97: 575–585.
7. Blennerhassett, M. G., M. Tomioka, and J. Bienenstock. 1991. Formation of contacts between mast cells and sympathetic neurons in vitro. *Cell Tissue Res.* 265: 121–128.
8. Stead, R. H., M. Tomioka, G. Quinonez, G. T. Simon, S. Y. Felten and J. Bienenstock. 1987. Intestinal mucosal mast cells in normal and nematode-infected rat intestines are in intimate contact with peptidergic nerves. *Proc. Natl. Acad. Sci. USA* 84: 2975–2979.
9. Keller, J. T., and C. F. Marfurt. 1991. Peptidergic and serotoninergic innervation of the rat dura mater. *J. Comp. Neurol.* 309: 515–534.
10. Krumins, S. A., and C. A. Broomfield. 1993. C-terminal substance P fragments elicit histamine release from a murine mast cell line. *Neuropeptides* 24: 5–10.
11. Cooke, H. J., P. Fox, L. Alferes, C. C. Fox, and S. A. Wolfe, Jr. 1998. Presence of NK1 receptors on a mucosal-like mast cell line, RBL-2H3 cells. *Can. J. Physiol. Pharmacol.* 76: 188–193.
12. van der Kleij, H. P., D. Ma, F. A. Redegeld, A. D. Kraneveld, F. P. Nijkamp, and J. Bienenstock. 2003. Functional expression of neurokinin 1 receptors on mast cells induced by IL-4 and stem cell factor. *J. Immunol.* 171: 2074–2079.
13. De Jonge, F., A. De Laet, L. Van Nassauw, J. K. Brown, H. R. Miller, P. P. van Bogaert, J. P. Timmermans, and A. B. Kroese. 2004. In vitro activation of murine DRG neurons by CGRP-mediated mucosal mast cell degranulation. *Am. J. Physiol. Gastrointest. Liver Physiol.* 287: G178–G191.
14. Dimtriadou, V., M. G. Buzzi, M. A. Moskowitz, and T. C. Theoharides. 1991. Trigeminal sensory fiber stimulation induces morphological changes reflecting secretion in rat dura mater mast cells. *Neuroscience* 44: 97–112.
15. Frieling, T., H. J. Cooke, and J. D. Wood. 1991. Serotonin receptors on submucous neurons in guinea pig colon. *Am. J. Physiol.* 261: G1017–G1023.
16. Frieling, T., H. J. Cooke, and J. D. Wood. 1993. Histamine receptors on submucous neurons in guinea pig colon. *Am. J. Physiol.* 264: G74–G80.
17. Corvera, C. U., O. Déry, K. McConalogue, P. Gamp, M. Thoma, B. Al-Ani, G. H. Caughey, M. D. Hollenberg, and N. W. Bunnett. 1999. Thrombin and mast cell tryptase regulate guinea-pig myenteric neurons through proteinase-activated receptors-1 and -2. *J. Physiol.* 517: 741–756.
18. Leon, A., A. Buriani, R. Dal Toso, M. Fabris, S. Romanello, L. Aloe, and R. Levi-Montalcini. 1994. Mast cells synthesize, store, and release nerve growth factor. *Proc. Natl. Acad. Sci. USA* 91: 3739–3743.
19. van Houwelingen, A. H., M. Kool, S. C. de Jager, F. A. Redegeld, D. van Heuven-Nolsen, A. D. Kraneveld, and F. P. Nijkamp. 2002. Mast cell-derived TNF-α primes sensory nerve endings in a pulmonary hypersensitivity reaction. *J. Immunol.* 168: 5297–5302.
20. Theoharides, T. C. 1996. The mast cell: a neuroimmunoendocrine master player. *Int. J. Tissue React.* 18: 1–21.
21. Theoharides, T. C., and D. E. Cochrane. 2004. Critical role of mast cells in inflammatory diseases and the effect of acute stress. *J. Neuroimmunol.* 146: 1–12.
22. Barbara, G., V. Stanghellini, R. De Giorgio, C. Cremon, G. S. Cottrell, D. Santini, G. Pasquinelli, A. M. Morselli-Labate, E. F. Grady, N. W. Bunnett, et al. 2004. Activated mast cells in proximity to colonic nerves correlate with abdominal pain in irritable bowel syndrome. *Gastroenterology* 126: 693–702.
23. Furuno, T., D. Ma, H. P. van der Kleij, M. Nakanishi, and J. Bienenstock. 2004. Bone marrow-derived mast cells in mice respond in co-culture to scorpion venom activation of superior cervical ganglion neurites according to level of expression of NK-1 receptors. *Neurosci. Lett.* 372: 185–189.
24. Suzuki, A., R. Suzuki, T. Furuno, R. Teshima, and M. Nakanishi. 2004. N-cadherin plays a role in the synapse-like structures between mast cells and neurites. *Biol. Pharm. Bull.* 27: 1891–1894.
25. Furuno, T., A. Ito, Y. Koma, K. Watabe, H. Yokozaki, J. Bienenstock, M. Nakanishi, and Y. Kitamura. 2005. The spermatogenic Ig superfamily/synaptic cell adhesion molecule mast-cell adhesion molecule promotes interaction with nerves. *J. Immunol.* 174: 6934–6942.
26. Ito, A., T. Jippo, T. Wakayama, E. Morii, Y. Koma, H. Onda, H. Nojima, S. Iseki, and Y. Kitamura. 2003. SgIGSF: a new mast-cell adhesion molecule used for attachment to fibroblasts and transcriptionally regulated by MITF. *Blood* 101: 2601–2608.
27. Koma, Y., A. Ito, T. Wakayama, K. Watabe, M. Okada, N. Tsubota, S. Iseki, and Y. Kitamura. 2004. Cloning of a soluble isoform of the SgIGSF adhesion molecule that binds the extracellular domain of the membrane-bound isoform. *Oncogene* 23: 5687–5692.
28. Kuramochi, M., H. Fukuhara, T. Nobukuni, T. Kanbe, T. Maruyama, H. P. Ghosh, M. Pletcher, M. Isomura, M. Onizuka, T. Kitamura, et al. 2001. TSLC1 is a tumor-suppressor gene in human non-small-cell lung cancer. *Nat. Genet.* 27: 427–430.
29. Yageta, M., M. Kuramochi, M. Masuda, T. Fukami, H. Fukuhara, T. Maruyama, M. Shibuya, and Y. Murakami. 2002. Direct association of TSLC1 and DAL-1, two distinct tumor suppressor proteins in lung cancer. *Cancer Res.* 62: 5129–5133.
30. Shingai, T., W. Ikeda, S. Kakunaga, K. Morimoto, K. Takekuni, S. Itoh, K. Satoh, M. Takeuchi, T. Imai, M. Monden, and Y. Takai. 2003. Implications of nectin-like molecule-2/IGSF4/RA175/SgIGSF/TSLC1/SynCAM1 in cell-cell adhesion and transmembrane protein localization in epithelial cells. *J. Biol. Chem.* 278: 35421–35427.
31. Fukuhara, H., M. Masuda, M. Yageta, T. Fukami, M. Kuramochi, T. Maruyama, T. Kitamura, and Y. Murakami. 2003. Association of a lung tumor suppressor TSLC1 with MPP3, a human homologue of *Drosophila* tumor suppressor *Dlg*. *Oncogene* 22: 6160–6165.
32. Masuda, M., M. Yageta, H. Fukuhara, M. Kuramochi, T. Maruyama, A. Nomoto, and Y. Murakami. 2002. The tumor suppressor protein TSLC1 is involved in cell-cell adhesion. *J. Biol. Chem.* 277: 31014–31019.

33. Takai, Y., J. Miyoshi, W. Ikeda, and H. Ogita. 2008. Nectins and nectin-like molecules: roles in contact inhibition of cell movement and proliferation. *Nat. Rev. Mol. Cell Biol.* 9: 603–615.
34. Biederer, T. 2006. Bioinformatic characterization of the SynCAM family of immunoglobulin-like domain-containing adhesion molecules. *Genomics* 87: 139–150.
35. Hagiyama, M., N. Ichiyanagi, K. B. Kimura, Y. Murakami, and A. Ito. 2009. Expression of a soluble isoform of cell adhesion molecule 1 in the brain and its involvement in directional neurite outgrowth. *Am. J. Pathol.* 174: 2278–2289.
36. Hosokawa, Y., M. Hagiyama, T. Iino, Y. Murakami, and A. Ito. 2011. Noncontact estimation of intercellular breaking force using a femtosecond laser impulse quantified by atomic force microscopy. *Proc. Natl. Acad. Sci. USA* 108: 1777–1782.
37. Yamada, D., M. Yoshida, Y. N. Williams, T. Fukami, S. Kikuchi, M. Masuda, T. Maruyama, T. Ohta, D. Nakae, A. Maekawa, et al. 2006. Disruption of spermatogenic cell adhesion and male infertility in mice lacking TSLC1/IGSF4, an immunoglobulin superfamily cell adhesion molecule. *Mol. Cell. Biol.* 26: 3610–3624.
38. Ito, A., M. Hagiyama, J. Oonuma, Y. Murakami, H. Yokozaki, and M. Takaki. 2007. Involvement of the SgIGSF/Necl-2 adhesion molecule in degranulation of mesenteric mast cells. *J. Neuroimmunol.* 184: 209–213.
39. Koma, Y., A. Ito, K. Watabe, T. Hirata, M. Mizuki, H. Yokozaki, T. Kitamura, Y. Kanakura, and Y. Kitamura. 2005. Distinct role for *c-kit* receptor tyrosine kinase and SgIGSF adhesion molecule in attachment of mast cells to fibroblasts. *Lab. Invest.* 85: 426–435.
40. Ito, A., M. Okada, K. Uchino, T. Wakayama, Y. Koma, S. Iseki, N. Tsubota, Y. Okita, and Y. Kitamura. 2003. Expression of the TSLC1 adhesion molecule in pulmonary epithelium and its down-regulation in pulmonary adenocarcinoma other than bronchioloalveolar carcinoma. *Lab. Invest.* 83: 1175–1183.
41. Koma, Y., T. Furuno, M. Hagiyama, K. Hamaguchi, M. Nakanishi, M. Masuda, S. Hirota, H. Yokozaki, and A. Ito. 2008. Cell adhesion molecule 1 is a novel pancreatic-islet cell adhesion molecule that mediates nerve-islet cell interactions. *Gastroenterology* 134: 1544–1554.
42. Okabe, S., C. Vicario-Abejón, M. Segal, and R. D. McKay. 1998. Survival and synaptogenesis of hippocampal neurons without NMDA receptor function in culture. *Eur. J. Neurosci.* 10: 2192–2198.
43. Suzuki, R., T. Furuno, D. M. McKay, D. Wolvers, R. Teshima, M. Nakanishi, and J. Bienenstock. 1999. Direct neurite-mast cell communication in vitro occurs via the neuropeptide substance P. *J. Immunol.* 163: 2410–2415.
44. Betz, W. J., F. Mao, and C. B. Smith. 1996. Imaging exocytosis and endocytosis. *Curr. Opin. Neurobiol.* 6: 365–371.
45. Tamura, A., K. Ozawa, T. Ohya, N. Tsuyama, E. M. Eyring, and T. Masujima. 2006. Nanokinetics of drug molecule transport into a single cell. *Nanomedicine (Lond)* 1: 345–350.
46. Hosokawa, Y., J. Takabayashi, S. Miura, C. Shukunami, Y. Hiraki and H. Masuhara. 2004. Nondestructive isolation of single cultured animal cells by femtosecond laser-induced shockwave. *Appl. Phys. A-Mater.* 79: 795–798.
47. Jiang, Y., Y. Matsumoto, Y. Hosokawa, H. Masuhara, and I. Oh. 2007. Trapping and manipulation of a single micro-object in solution with femtosecond laser-induced mechanical force. *Appl. Phys. Lett.* 90: 061107.
48. Koyasu, S., H. Nakauchi, K. Kitamura, S. Yonehara, K. Okumura, T. Tada, and I. Yahara. 1985. Production of interleukin 3 and γ-interferon by an antigen-specific mouse suppressor T cell clone. *J. Immunol.* 134: 3130–3136.
49. Dehay, C., and H. Kennedy. 2007. Cell-cycle control and cortical development. *Nat. Rev. Neurosci.* 8: 438–450.
50. Maurel, P., S. Einheber, J. Galinska, P. Thaker, I. Lam, M. B. Rubin, S. S. Scherer, Y. Murakami, D. H. Gutmann, and J. L. Salzer. 2007. Nectin-like proteins mediate axon Schwann cell interactions along the internode and are essential for myelination. *J. Cell Biol.* 178: 861–874.
51. Fogel, A. I., M. R. Akins, A. J. Krupp, M. Stagi, V. Stein, and T. Biederer. 2007. SynCAMs organize synapses through heterophilic adhesion. *J. Neurosci.* 27: 12516–12530.
52. Hashimoto, K., R. Ichikawa, K. Kitamura, M. Watanabe, and M. Kano. 2009. Translocation of a "winner" climbing fiber to the Purkinje cell dendrite and subsequent elimination of "losers" from the soma in developing cerebellum. *Neuron* 63: 106–118.
53. Tanabe, Y., T. Kasahara, T. Momoi, and E. Fujita. 2008. Neuronal RA175/SynCAM1 isoforms are processed by tumor necrosis factor-α-converting enzyme (TACE)/ADAM17-like proteases. *Neurosci. Lett.* 444: 16–21.
54. Taiwo, O. B., K. J. Kovács, and A. A. Larson. 2005. Chronic daily intrathecal injections of a large volume of fluid increase mast cells in the thalamus of mice. *Brain Res.* 1056: 76–84.
55. Hendrix, S., K. Warnke, F. Siebenhaar, E. M. Peters, R. Nitsch, and M. Maurer. 2006. The majority of brain mast cells in B10.PL mice is present in the hippocampal formation. *Neurosci. Lett.* 392: 174–177.
56. Nautiyal, K. M., A. C. Ribeiro, D. W. Pfaff, and R. Silver. 2008. Brain mast cells link the immune system to anxiety-like behavior. *Proc. Natl. Acad. Sci. USA* 105: 18053–18057.
57. Ito, A., M. Hagiyama, and J. Oonuma. 2008. Nerve-mast cell and smooth muscle-mast cell interaction mediated by cell adhesion molecule-1, CADM1. *J. Smooth Muscle Res.* 44: 83–93.